2007

Assessment Of Dynamic Contrast Enhanced MRI For The Early Detection Of Treatment Response In Human Advanced Hepato-Cellular Carcinoma

Yun Jiang
University of Alabama at Birmingham

ASSESSMENT OF DYNAMIC CONTRAST ENHANCED MRI FOR THE EARLY DETECTION OF TREATMENT RESPONSE IN HUMAN ADVANCED HEPATO-CELLULAR CARCINOMA

by

YUN JIANG

THIAN C. NG, COMMITTEE CHAIR
JAMES A. POSEY III
DONALD B. TWIEG

A THESIS

Submitted to the graduate faculty of The University of Alabama at Birmingham,
in partial fulfillment of the requirements for the degree of
Master of Science

BIRMINGHAM, ALABAMA

2007

ASSESSMENT OF DYNAMIC CONTRAST-ENHANCED MRI FOR THE EARLY DETECTION OF TREATMENT RESPONSE IN HUMAN ADVANCED HEPATO-CELLULAR CARCINOMA

YUN JIANG

BIOMEDICAL ENGINEERING

ABSTRACT

Dynamic contrast-enhanced magnetic resonance imaging (DCE-MRI) has been shown to be a potentially useful tool for early prediction of tumor response to anti-angiogenesis agents. In this study, the technique was used to evaluate the chemotherapeutic drug doxorubicin with or without the tyrosine kinase inhibitor sorafenib in patients with advanced hepatocellular carcinoma (HCC).

Five male patients (ages 50 to 78 years, average age 67 ± 8 years) were studied with serial T_1-weighted DCE-MRI to measure the alteration of perfusion parameters of tumors in response to the treatment. All patients received doxorubicin at dose of 60 mg/m^2 intravenously every 21 days. Among them, 3 patients also received sorafenib 400 mg orally twice daily, and 2 patients (control) received placebos. DCE-MRI studies at 3 T were performed one day before, and one week, 6 weeks and 12 weeks after therapies were started. The initial enhancement rate (E_R) was calculated, and a general kinetic model was employed to fit the signal enhancement curve to generate the volume transfer constant (K^{trans}).

Histogram and mean perfusion analyses showed that both perfusion parameters K^{trans} and E_R in HCC tumors of the 3 patients receiving sorafenib and doxorubicin shifted to a lower cellular population distribution the first week after treatment and showed that the profiles of a large population distribution in low values remained similar at 6 and 12

weeks after treatments were started; These findings suggest that the antiangiogenic agent sorafenib is effective in these cases. One of these patients showed significant mass reduction during this study. For this patient, the mean values of E_R and K^{trans} over the whole tumor region obtained before treatment and one week after treatment was begun were found to decrease from 0.23 s^{-1} to 0.15 s^{-1} and from 0.14 s^{-1} to 0.02 s^{-1}, respectively. One patient treated with only doxorubicin exhibited significant decrease in perfusion parameters, a result suggesting that this drug may have had an antiangiogenic effect in this patient.

I have successfully accomplished both the implementation of *in vivo* DCE-MRI acquisition with the use of a high field 3T clinical scanner and the postprocessing of multiple vascular and perfusion parameters with the use of the Matlab platform. The DCE-MRI results from the studies of HCC patients demonstrate that DCE-MRI is a sensitive biomarker for the early detection of the efficacy of antiangiogenic drugs.

ACKNOWLEDGMENTS

First, I thank my mentor, Dr. Thian C. Ng. In the past several years, Dr. Ng has given me excellent guidance and continuous encouragement on my *in vivo* MRI studies in human patients. Besides advising me in matters related to my research project, Dr. Ng also inspired me in my managing of career growth.

My deep gratitude is also extended to the members of my thesis committee, Drs. James A Posey III and Donald B. Tweig, for their continuing support, comments, and fruitful discussions. I thank Dr. Posey for kindly allowing me to do this project and for teaching me about human hepatocellular carcinoma. My special thanks go to Dr. Twieg, who interviewed me 5 years ago and gave me the opportunity to explore my research interest at The University of Alabama at Birmingham.

I am grateful to all faculty members, students and staffs of the Department of Biomedical Engineering, for their helps during this thesis work. My special appreciation is also extended to Ms. Thyrza Johnson for her assistance throughout these years.

In addition, I express my sincere love to my wife, Wanfeng Yu, and my deep appreciation of her encouragement and support. I also thank my parents, Hengchang Jiang and Huiying Wang, and my parents-in-law, Qiying Yu and Pengyuan Wan, for their understanding and support.

TABLE OF CONTENTS

Page

TABLE OF CONTENTS (Continued)

Page

LIST OF FIGURES

Figure *Page*

LIST OF ABBREVIATIONS

AIF	arterial input function
CNS	central nervous system
DCE-MRI	dynamic contrast-enhanced magnetic resonance imaging
ECOG	Eastern Cooperative Oncology Group
EES	extracellular extravascular space
E_R	initial enhancement rate
ERK	extracellular signal-regulated kinase
FFE	fast field echo
FOV	field of view
Gd	gadolinium
Gd-DTPA	gadolinium diethyltriaminepentaacetic acid
GKM	general kinetic model
HCC	hepatocellular carcinoma
HIV	human immunodeficiency virus
K^{trans}	volume transfer constant
k_{ep}	flux rate constant between extracellular extravascular space and plasma
M_0	equilibrium magnetization
MAP	mitogen-activated protein
MEK	mitogen-activated protein and extracellular signal-regulated kinase

MR	magnetic resonance
MRI	magnetic resonance imaging
PDGFR-β	platelet-derived growth factor receptor beta
r_1	spin-lattice relaxivity
r_2	spin-spin relaxivity
RECIST	response evaluation criteria in solid tumors
ROI	region of interest
SENSE	sensitivity-encoding
T_1	longitudinal relaxation time
T_{10}	precontrast longitudinal relaxation time
T_2	transverse relaxation time
T_2^*	net transverse relaxation time
TE	echo time
TR	repetition time
TSE	turbo spin echo
VEGF	vascular endothelial growth factor
VEGFR	vascular endothelial growth factor receptor
VEGFR-2/-3	vascular endothelial growth factor receptor-2/-3
v_e	volume of extracellular extravascular space per unit volume of tissue
VPF	vascular permeability factor

INTRODUCTION

Hepatocellular Carcinoma

Hepatocellular carcinoma (HCC), which is the most common primary hepatic tumor, the fifth most common malignancy, and the second most fatal cancer worldwide (1), represents over 5% of all cancers. From 500,000 to one million new cases are reported each year worldwide (2), and these cases generally lead to death within 6-20 months. HCC is more common in developing countries and in areas such as Asia and sub-Saharan Africa because of the high rate of hepatitis B and C infections. However, the incidence of HCC has been rising in the West, largely as a result of liver cirrhosis and high alcohol consumption. Surgical resection or transplantation of the liver is considered the best strategy for treating HCC but only can be applied to a minority of patients (possibly 5%–15%) whose disease is at an early stage (3). When surgery or transplantation is not possible, systemic chemotherapy is normally employed to prolong survival. Most single agent traditional systemic therapy has never shown any survival benefit in the treatment of HCC (4) because of the high frequency of overexpressed drug resistance gene in HCC and because of the difficulty in delivering some chemotherapy agents as a result of liver cirrhosis and liver dysfunction. Therefore, there is an urgent need for novel strategies for the treatment of advanced HCC, such as antiangiogenic treatment or traditional systemic therapy combined with novel targeted therapy relevant to antiangiogenesis and inhibition of cellular proliferation.

Overview of Angiogenesis

What Is Angiogenesis?

Angiogenesis is the multistep process of the formation of new blood vessels and is controlled by a series of signaling chemicals, angiogenesis activators, and angiogenesis inhibitors. When more angiogenesis activators than angiogenesis inhibitors are released, the net result is the generation of more new vessels. If more angiogenesis inhibitors are presented, angiogenesis is inhibited, and vessel density reduces. Angiogenesis occurs normally in the human body at specific times in development and growth (e.g., during fetal development), when new vessels for the growing body need to be created. In the healthy adult, angiogenesis process is "turned off" by the release of more inhibitors than growth factors, except for the repair and regeneration of tissue during wound healing and during the menstrual cycle.

Tumor Angiogenesis

Tumor angiogenesis is the proliferation of a network of blood vessels that penetrates into the tissue area of cancerous growths, supplying nutrients and oxygen and removing waste products. In the early stages of a tumor's growth, the tumor can be sustained by passive diffusion of nutrients and oxygen. However, a tumor requires a direct blood supply to sustain its growth once its volume becomes larger than 2-3 mm^3 (5). Tumor angiogenesis starts with cancerous tumor cells releasing angiogenesis activators that send signals to stimulate formation of new vessels in the surrounding normal host tissue. It has been found that more than a dozen different proteins and several smaller molecules work as angiogenesis activators released by tumors. Among them, vascular endothelial growth

factor (VEGF), also known as vascular permeability factor (VPF), appears to be the most important for sustaining tumor growth. VEGF, which has many subtypes and is synthesized inside tumor cells, diffuses into the surrounding tissue and binds to vascular endothelial growth receptors (VEGFRs) on the endothelial cells. This binding activates multiple signal transduction pathways, including phosphorylation of tyrosine kinases, protein kinases, and MAP kinases, and the result is endothelial gene expression and cell proliferation (6-8), which leads to a series of processes that result in the formation of new blood vessels for tumor cell proliferation.

Antiangiogenesis

It has been shown by Folkman (5) that angiogenesis plays a key factor in the growth and spread of tumors. "Antiangiogenesis" is thus aimed at halting cancer progression by suppressing the tumor blood supply, and is becoming a new therapeutic strategy in modern clinical oncology. This approach has proved attractive because it starves a larger number of tumor cells by targeting a smaller number of endothelial cells. This new strategy may reduce the drug resistance problem because the tumor cell is not directly targeted. Antiangiogenesis therapy for cancer has developed rapidly since the first clinical trial of an angiogenesis inhibitor in 1992. Since then, a wide variety of agents, termed *antiangiogenesis drugs*, have been discovered. There are dozens of these agents in clinical trial, and hundreds more are in preclinical evaluation. These molecules target one or more steps in the angiogenic signaling cascade to inhibit the formation of tumor blood vessels; for example, anti-VEGF antibodies block the VEGFR from binding with the growth factor. One property of VEGF is promotion of vascular endothelial permeability, so the permea-

bility of tumor vasculature would be reduced once the VEGF signaling pathway was inhibited.

Unlike traditional systemic therapies, most antiangiogenic drugs are cytostatic rather than cytotoxic. They do not show acute dose-limiting toxicity and are more likely to produce tumor stabilization instead of tumor response. Clearly, the challenge in the clinical development of antiangiogenic therapeutic drugs is to look for powerful biomarkers to detect the treatment response of these drugs early and possibly optimize the effectiveness of these compounds. Dynamic contrast-enhanced MRI (DCE-MRI) offers the ability to noninvasively detect changes in tumor perfusion, vascular membrane permeability, flow rates, and extracellular extravascular space (EES). Pharmacokinetic parameters measured by DCE-MRI could potentially be important biomarkers for clinical development of antiangiogenic drugs.

DCE-MRI

DCE-MRI acquires sequential T_1-weighted images before, during, and after the administration of a contrast agent (e.g., gadolinium diethyltriaminepentaacetic acid [Gd-DTPA]). This method has shown great potential in oncology applications, in which *in vivo* information about physiological properties such as vessel permeability, blood flow, blood volume, and extracellular extravascular volume is required (9). The use of DCE-MRI has been widely reported in studies of various cancers, such as brain cancer (10-13), breast cancer (14,15), rectal cancer (16), urinary bladder and prostate cancer (17), cervical carcinoma (18), and colorectal liver metastases (19). The technique has been used to monitor the effects of a variety of treatments. Barentsz et al. (20) and van Larrhoven et

al. (21) reported that pharmacokinetic parameters of DCE-MRI could be early predictors of chemotherapeutic response. Hawighorst et al. (22) showed that it was possible to assess malignant glioma response to stereotactic radiotherapy by determining the degree of signal enhancement and the exchange rate constant of DCE-MRI. Padhani et al. (23) used DCE-MRI to assess the effects of androgen deprivation on prostate cancer. Posey et al. (24) predicted the results of anti-kinase insert domain-containing receptor antibody therapy by measuring the influx volume transfer rate in liver metastases from colorectal carcinoma. In addition, it has been shown that DCE-MRI is a useful method for detecting tumor response to antiangiogenesis agents at an early stage (25).

Basis of Contrast-Enhanced MRI

It is known that malignant tumors exhibit more vascularity and higher endothelial permeability than normal or less aggressive malignant tissues do. Tumor vasculature is often highly heterogeneous, with poorly differentiated and fragile vessels. Capillary walls have bigger endothelial junctions and a discontinuous or absent basement membrane, which makes tumor capillaries extremely leaky (26). Thus, in contrast-enhanced MRI, malignant tumors generally have levels of enhancement that are faster and higher than those seen in normal tissue (27).

In a DCE-MRI study, contrast agent travels through the vascular system after intravenous bolus injection. The agent leaks from the vascular space to the EES by a passive diffusion process driven by contrast agent concentration differences. Thus, contrast agent will accumulate in the EES. Because of tissue leakage and renal excretion, contrast agent concentration in the vascular space will then drop to a level lower than the

concentration in the EES, and the result is backflow from the EES to the plasma space until all of the contrast agent is eliminated (28).

Gadolinium-chelate is commonly used in clinical MRI for diagnosis. Gadolinium (Gd) has unpaired electron spins in its outer shells and has long relaxivity. This magnetic metallic element disturbs both the longitudinal relaxation rate and the transverse relaxation rate of protons in tissues where it binds. According to the Solomon-Bloembergen equation, the change in relaxation rates ($1/T_1$ and $1/T_2$) is directly proportional to the concentration of Gd ions. The relationship between relaxation rate and concentration of contrast agent is as follows:

$$\frac{1}{T_1} = \frac{1}{T_{10}} + r_1[Gd] \quad (1)$$

$$\frac{1}{T_2} = \frac{1}{T_{20}} + r_2[Gd] \quad (2)$$

where r_1 and r_2 are spin-lattice and spin-spin relaxivities of the contrast agent, respectively, and T_{10} and T_{20} are precontrast longitudinal relaxation time and precontrast transverse relaxation time, respectively. Relaxivities represent the ability of the contrast agent to change the relaxation rates of the surrounding water proton spins to an extent.

From Equation 1, it can be seen that the change in Gd concentration affects the T_1 value of the water proton signal in a tissue. Because a change in the T_1 value alters the signal intensity acquired by a T_1-weighted imaging sequence, a series of T_1-weighted images is able to monitor the change in contrast agent concentration. Figure 1 shows a simulated of signal intensity versus time curve acquired by a series of T_1-weighted images; the signal-to-time enhancement curve from a malignant tumor (red curve) has stronger and faster wash-in enhancement rates and a faster wash-out rate than the curve of normal tissue

(black curve) does. The figure shows the MR signal intensities from each time point of before (line 1 to line 2), during (line 2 to line 3), and after (line 3 to line 4) the injection of the contrast agent.

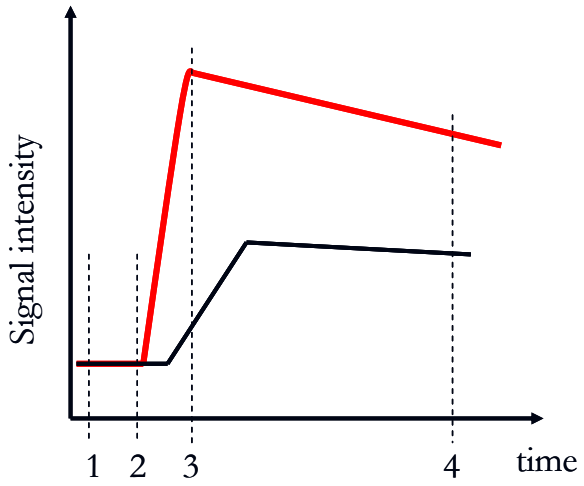

Figure 1. Image signal intensities of each time point during the contrast agent movement acquired by a T_1-weighted pulse sequence.

The signal enhancement observed in DCE-MRI is affected by several mechanisms, including variations of regional blood flow, proportional blood vessel density, regional variations in haematocrit, proportional vascularization of existing blood vessels, variations in the surface area permeability of the endothelial membranes, and the contrast agent concentration difference existing between plasma and the EES (28). Folkman (5) suggested that highly active angiogenesis exists in a rapidly growing tumor to support its nutrition and oxygen demands and that more aggressive tumors display increased angiogenesis-related microvasculature abnormalities. On the basis of the characteristics of contrast enhancement of DCE-MRI, the dynamic of flow and the vascular permeability can be quantified to measure the angiogenic activity at the cellular and molecular levels. The

efficacy of drug regimen designed to diminish the tumor angiogenesis can thus be measured with DCE-MRI noninvasively and repeatedly.

DCE-MRI Acquisition Techniques

A variety of pulse sequences is available in most clinical MRI scanners. Sequences for acquiring DCE-MRI data are always compromised among temporal resolution, speed, and image quality. DCE-MRI requires the pulse sequence to have a fast measurement rate, sufficient dynamic range to monitor the rapid change of contrast agent concentration-dependent signals within tumors, and large spatial coverage of the tissue. Modern commercial systems offer optimized keyhole or parallel imaging techniques that can increase temporal resolution to 6 fold in a 3D spatial coverage, making those techniques very attractive for DCE-MRI (29,30).

T_1-weighted DCE-MRI is most commonly acquired by a gradient echo sequence with spoiling of the transverse magnetization. The signal intensity is described (31) as

$$S_0 = M_0 e^{-TE/T_2^*} \sin\theta \left(\frac{1 - e^{-TR/T_1}}{1 - \cos\theta e^{-TR/T_1}} \right) \qquad (3)$$

where M_0 is the equilibrium magnetization; θ is the flip angle; TR and TE are the repetition time and echo time, respectively, in the pulse sequence used; and T_2^* is the net transverse relaxation time. If it is assumed that $TR \cdot r_1 \cdot C_t << 1$, $TE \cdot r_2 \cdot C_t << 1$, and $TR << T_{10}$, which is normally the case for low Gd-DTPA concentrations (32), the signal enhancement after the bolus injection of contrast agent can be expressed as

$$\frac{S(t) - S_0}{S_0} \approx T_{10} \cdot r_1 \cdot C_t(t) \qquad (4)$$

where $S(t)$ represents the signal intensity after the injection of the contrast agent at each time point. Equation 4 establishes a linear relationship between the concentration of contrast agent and the signal enhancement acquired by a gradient echo sequence.

Pharmacokinetic Model

The quantitative measurement of the physiological properties of tissue requires a certain pharmacokinetic model with which to understand the tissue characterization of signal enhancement in the EES. Simple pharmacokinetic models of tissue have been used to calculate parameters such as the volume transfer constant (K^{trans}), the flux rate constant between the extracellular extravascular space and plasma (k_{ep}), and the volume of extracellular extravascular space per unit volume of tissue (v_e) (33). By following the two compartment model described by Tofts and Kermode (34) and Larsson et al. (11), Daldrup et al.(14) employed a general kinetic model (GKM) to understand the kinetics of contrast enhancement. The GKM divides the anatomy of the tumor or tissue into two functional components, the vascular space and the EES, and one nonfunctional component, the intracellular space. Figure 2 shows the diagram of the GKM.

The net change in the tissue can be described as follows:

$$\frac{dC_t}{dt} = K^{trans} C_p - k_{ep} C_t \qquad (5)$$

where C_t is the tissue concentration of the contrast agent, C_p is the concentration of the contrast agent in plasma, and $v_e = K^{trans}/k_{ep}$. Furthermore, Equation 5 can be described as a convolution integral.

$$C_t(t) = K^{trans} \cdot e^{-k_{ep}t} \otimes C_p(t) \qquad (6)$$

where $\otimes$ represents the convolution operation. K^{trans} and k_{ep} can be obtained by a nonlinear curve-fitting algorithm based on Equation 6.

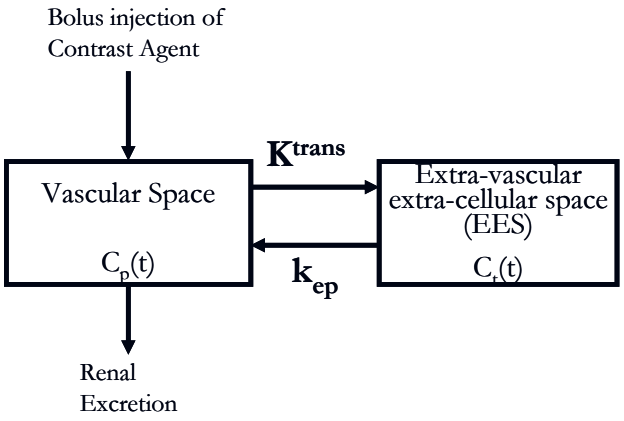

Figure 2. Diagram of general kinetic model.

In the simplest model of the signal enhancement in the DCE-MRI, three parameters are commonly used: the maximum signal enhancement, the initial enhancement rate, and the rate when the signal decays during "wash-out." When these three parameters are used, it is assumed that the concentration of the contrast agent reaches equilibrium in the plasma immediately after injection of the contrast agent, and dynamic concentration change in the vascular system is ignored. However, it is important to consider the contribution of plasma in the DCE-MRI modeling because plasma perfuses the tissue.

DCE-MRI in the Liver

The liver has a unique vascular anatomy, which receives both arterial blood from the systemic circulation via the hepatic arteries and a larger venous blood flow from the bowel and spleen via the hepatic portal system. It is important to consider this dual blood

supply in the investigation of hepatic diseases. The quantification of hepatic perfusion parameters necessitates that the proportional contribution of these two inputs to each voxel of tissue be known. Unfortunately, it is not clear what fractional distributions of blood supply are delivered from arteries and portal veins to the tissue, especially in those patients with advanced liver disease. Another complication is that the liver lies directly below the diaphragm and is subjected to extreme respiratory motion. The motion artifacts within the time course in DCE-MRI acquisition are highly undesirable because pharmacokinetic modeling assumes that the signal change observed in the time course is from the same voxel of tissue. Therefore, DCE-MRI of the liver requires an optimized imaging protocol or pharmacokinetic model to meet the particular demands.

In the liver, the portal vein phase generally begins 20-30 seconds after the arterial phase (35), so it can be assumed that the early signal enhancement curve in DCE-MRI reflects only the arterial blood supply instead of the dual blood supply. A modern clinical MR scanner is able to acquire a 3D coverage in 1-2 seconds, which will yield sufficient time points to calculate kinetic parameters. In our study, a breath-holding technique was used in for duration of the DCE-MRI acquisition. The first 30 seconds of the signal enhancement curve (with the patient holding the breath) were used to calculate K^{trans} to avoid the blood contribution of the later portal vein phase to tissue and to minimize respiratory motion artifact.

Overview of Thesis

The main objective of this thesis project was to use DCE-MRI at 3 T to evaluate the effect of treatment of HCC during a clinical trial. It was necessary to set up a DCE-MRI

protocol in the liver; to acquire serial T_1-weighted images with contrast agent at pre-treatment, and at one week, 6 weeks, and 12 weeks during the treatment; and to implement the postprocessing software in Matlab (Mathworks Inc., MA USA) to analyze multiple perfusion parameters for studying whether the DEC-MRI provides significant perfusion biomarkers for early detection of the vascular changes in response to the tyrosine kinase inhibitor, sorafenib, which intercepts signaling pathways that are relevant to angiogenesis.

The thesis is divided into four main parts. Part 1 provides a brief description of HCC, tumor angiogenesis, antiangiogenesis, and DCE-MRI. Part 2 covers the method used in the data acquisition and analysis. Part 3 shows results from 5 patients, and Part 4 contains a discussion of the results.

MATERIALS AND METHODS

This study was approved by the Institutional Review Board for Human Use at The University of Alabama at Birmingham (see Appendix) and was conducted in accordance with US Department of Health and Human Services guidelines. Informed consent was obtained from each patient.

Patients' Eligibility

Patients with measurable, histologically proven, inoperable HCC who had not received prior systemic treatments for HCC were eligible for enrollment. Inclusion criteria included life expectancy of at least 12 weeks; Eastern Cooperative Oncology Group (ECOG) performance status of 0, 1, or 2; and tumor lesion measured in at least one dimension according to RECIST.

Patients were excluded who had a history of myocardial disease; serious myocardial dysfunction; active clinically serious infections; a known history of HIV infection; or known CNS tumors, including metastatic brain disease.

Treatment and Dose

All patients received doxorubicin 60 mg/m^2 intravenously every 21 days (one cycle), for a total dose of 360 mg/m^2 in the whole treatment period (six cycles). Patients got either sorafenib 400 mg or placebo orally twice daily.

Sorafenib

Sorafenib is a multikinase inhibitor that targets Raf/MEK/ERK signaling at the level of Raf kinase to block tumor cell proliferation and targets vascular endothelial growth factor receptor-2/-3 (VEGFR-2/-3) and platelet-derived growth factor receptor beta (PDGFR-β) tyrosine kinases to inhibit angiogenesis. Both angiogenesis and signaling through the Raf/MEK/ERK cascade play critical roles in the development of HCC (36). A previous phase I trial of sorafenib has confirmed partial response in a metastatic HCC patient (37). A phase II study of sorafenib in advanced HCC patients confirmed that 2.2% of patients achieved a partial response (38). These data led to the development of the current study, which was designed to examine the efficacy of using DCE-MRI for early detection of the effect of treatment with doxorubicin alone or with doxorubicin plus sorafenib in patients with advanced HCC.

Doxorubicin

Doxorubicin is a chemotherapy drug given as a treatment for many different types of cancer, such as breast cancer, lung cancer, and soft tissue sarcoma. The mechanism of action of doxorubicin is to inhibit the progression of the enzyme topoisomerase II. The drug stabilizes the topoisomerase II complex that breaks the DNA chain, to prevent the DNA double helix from being resealed and thereby to stop the process of DNA replication.

Doxorubicin is given by intravenous injection. Possible side effects include nausea, vomiting, heart arrhythmias, and alopecia (hair loss).

MRI Protocol

MRI studies were performed on a 3 T Philips Achieva MR scanner (Philips Medical System, Best, The Netherlands), with a body coil transmitter and a SENSE Torso receive coil. Patients were scheduled to have four MRI scans one day before, and one week, 6 weeks, and 12 weeks after starting therapies.

Normal T_1-weighted and T_2-weighted images were acquired to locate the tumor lesions in the liver. T_1-weighted image was acquired by T_1-weighted fast field echo (FFE) with TR/TE = 140/1.15 ms. The T_2-weighted image was acquired by T_2-weighted turbo spin echo (TSE) with fat saturation with TR/TE = 2000/70 ms. DCE-MRI data were acquired by a 3D T_1-weighted FFE sequence with a 15 degree flip angle. *TR* and *TE* were 5 ms and 2.3 ms, respectively. The field of view (FOV) was 400 × 280 × 60 mm with an acquisition matrix of 192 × 192 × 10, that was reconstructed to 256 × 256 × 10. The effective SENSE factor was 2. The pulse sequence produced a dynamic resolution of 2.1 seconds, an acquisition pixel size of 2.08 × 1.46 × 6 mm, and a reconstruction pixel size of 1.88 × 1.09 × 6 mm. The same sequence with a 5 degree flip angle was acquired before injection of the contrast agent to generate a precontrast T_1 map. A dosage of 0.1 mM/kg GD-DTPA (Magnevist; Berlex Laboratories, Wayne, NJ) was administered intravenously, followed by a 20 ml saline flush at a rate of 3 ml/sec by a powered injector at 42 seconds after starting acquisition. A total of 2000 images (200 dynamics repeat, 10 slices) were acquired over a period of 7 minutes. During the DCE-MRI scan, patients were asked at the start of the Gd-DTPA injection to hold their breath for as long as they could and then to either hold their breath periodically or breathe shallowly in accordance with their physical

conditions. In each follow-up study, the 3D slab was visually positioned the same as in the first study by reference to the spinal cord.

Data Analysis

Data were analyzed on Matlab platform on a Linux workstation. All 2000 dynamic images acquired in a session of study were loaded. For each patient, one slice covering the HCC of interest was selected for the calculation perfusion parameters; this procedure ensured that the same location from different sessions would be compared by reference to the spinal cord of each patient. Generally, the slice was selected to cover both the tumor lesion area and normal liver tissue.

A signal enhancement curve was obtained by subtracting the images $S(t)$ from the baseline image before the arrival of Gd-DTPA, S_0, and then dividing the subtraction images ($S(t) - S_0$) by the same baseline image. This baseline image was carefully selected to be acquired after the patient began breath holding but before contrast agent arrival.

The initial enhancement rate (E_R) of the signal enhancement curve equals the slope of the wash-in curve and was calculated by linear curve fit time points between the point just after the contrast agent arrival and the one of the maximum enhancement. E_R was calculated pixel by pixel over a region of interest (ROI) that was selected intentionally to cover the whole tumor lesion area for studies.

It is important to understand the tissue characterization of signal enhancement in the EES in terms of pharmacokinetic parameters. Many different pharmacokinetic models and perfusion parameters of physiological relevance have been proposed in the DCE-MRI. An extensive review has been made by Tofts et al. (33) in an attempt to unify perfusion

parameters. Concurring with those authors, we chose a two compartment GKM pharmacokinetic model with a notation of parameters that is similar to their suggestions. The schematic diagram of the GKM is shown in Figure 2 in the Introduction section of the thesis.

By combining Equation 4 and Equation 6, one arrives at the following equation:

$$\frac{S_t(t)}{S_0} - 1 \approx T_{10} \cdot r_1 \cdot K^{trans} \cdot e^{-k_{ep}t} \otimes C_p(t) \qquad (7)$$

A mean intensity of pixels of an ROI in the aorta was first calculated over serial dynamic images. Thus, mean intensity vs. time curve was generated as arterial input function (AIF). The AIF was modeled as a triexponential function:

$$C_p(t) = \sum_{i=1}^{3} e^{-\lambda_i (t - tlag)} \qquad (8)$$

where *tlag* is the contrast agent arrival time.

K^{trans} was calculated by applying a nonlinear curve-fitting algorithm to the first 30 seconds of the signal enhancement time curve in the same ROI used in the E_R calculation.

RESULTS

Five male patients met the inclusion criteria. Three of them completed all four MRI study sessions, and 2 patients completed the first three MRI studies. Patients' ages ranged from 50 to 78 years old (average age 67 ± 8 years).

Figure 3 shows axial abdomen images covering the liver of a representative patient (patient 3). A hepatocellular lesion can be observed in the right lobe of the liver. HCC may have a variety of signal patterns on T_1- and T_2-weighted images but in most cases shows a hypointense pattern on a T_1-weighted image and a hyperintense pattern on a T_2-weighted image, as shown in Figure 3a and 3b. HCCs are commonly hypervascular tumors that show enhancement in a diffuse heterogeneous fashion on immediate post-contrast-enhanced MR images (see Figure 3c). This important feature distinguishes malignant primary hepatocellular tumors from benign tumors that enhance homogeneously. From this post-contrast-enhanced image, several tumor nodules can be observed that were not shown in normal T_1- and T_2-weighted images. The enhancement image calculated on the basis of Equation 4 is shown in Figure 3d, with the baseline image subtracted from the image acquired 21 seconds later. ROIs were defined inside the tumor, in the tumor peripheral area, and in the relatively normal liver tissue. ROIs drawn in normal liver tissue were carefully selected to avoid tumor nodules and large vasculature in the liver.

The mean intensity in each ROI was calculated for each dynamic image over the 200 time points. Figure 4 shows the signal enhancement curves from ROIs (shown in

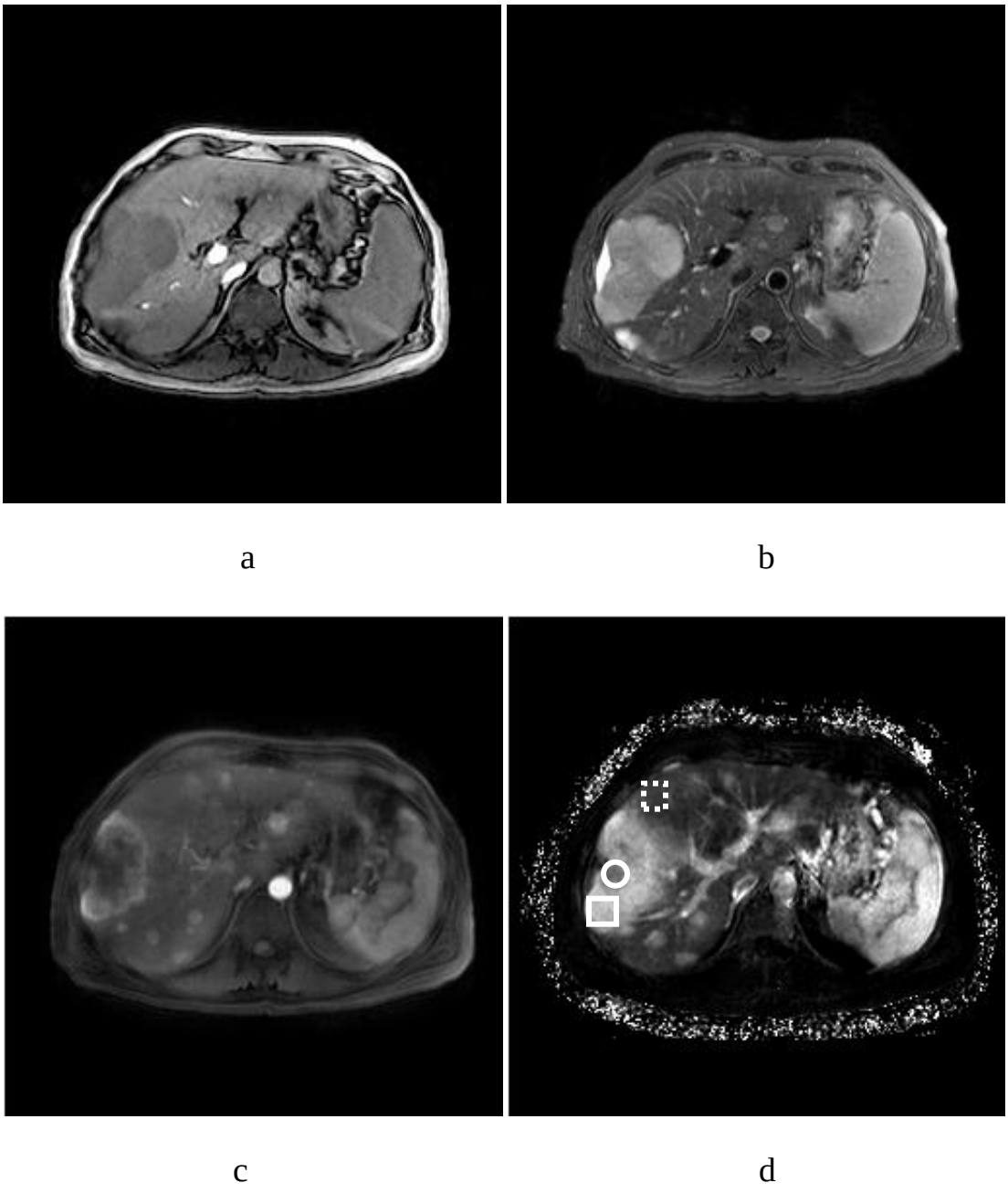

Figure 3. Axial abdomen images of a representative HCC patient. a: A T_1-weighted image clearly shows a tumor lesion at the right lobe of the liver. HCC demonstrates hypointensity in T_1-weighted image. b: T_2-weighted image shows hyperintensity for HCC. c: A diffuse heterogeneous enhancement was shown in an immediate postcontrast image acquired 10 seconds after injection of contrast agent was begun. d: The signal enhancement image, with the baseline image subtracted from the image acquired 21 seconds later. A solid square ROI in the tumor peripheral area, a solid circle ROI inside the tumor necrotic area, and a dashed square ROI in the relatively normal liver tissue were drawn to generate the signal enhancement vs. time curves shown in Figure 4.

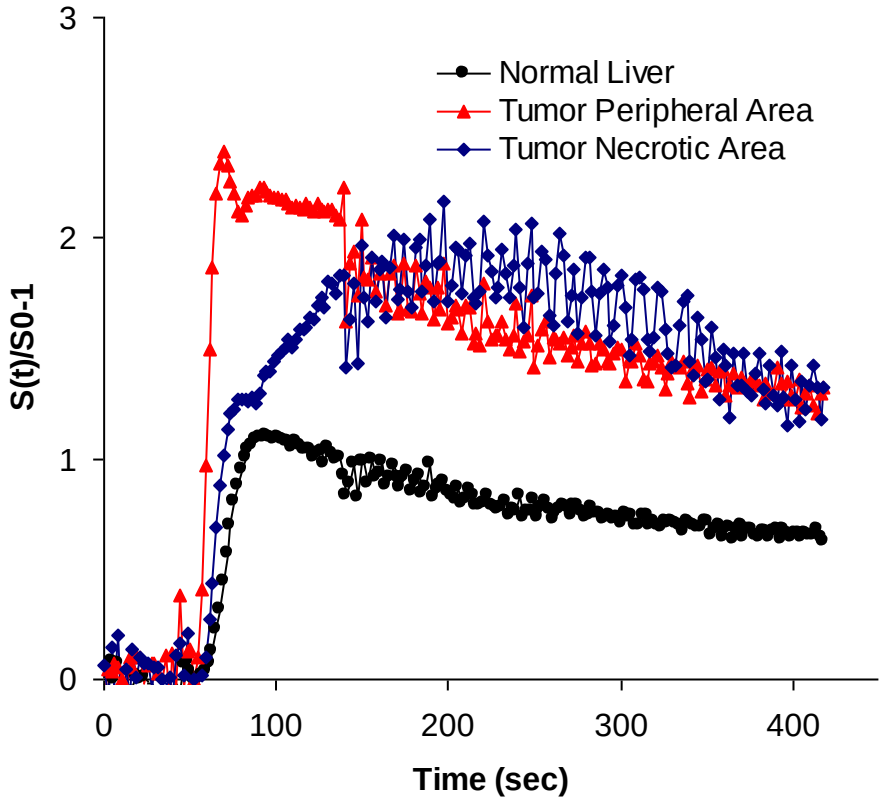

Figure 4. Signal enhancement vs. time curves from a representative patient. Signal enhancement was calculated based on Equation 2. The mean intensities of ROIs at different areas of each dynamic image over 200 time points were plotted. The wash-in slope is equal to the E_R.

Figure 3d) of different tissues from the same patient's data. Figure 3d clearly shows that there are differences in perfusion characteristics among different tissue types. The tumor peripheral area has faster and stronger enhancement than the other two regions do. A faster wash-out rate in the tumor peripheral region is also visualized. From these curves, it can be seen that the data began to be affected by motion artifact around 30 seconds after contrast agent arrival, at which the patient could not hold his breath any longer, and began to breathe shallowly.

The wash-in curve slope was calculated as the E_R. An ROI was drawn to cover the major tumor lesion. The wash-in curve slope was calculated pixel by pixel in the ROI to

generate the color map for visualization. A display of the ROI color map of E_R overlapping on the respective T_2-weighted anatomical image is shown in Figure 5. The tumor peripheral area shows a faster enhancement rate than the tumor necrotic area and the normal liver tissue do.

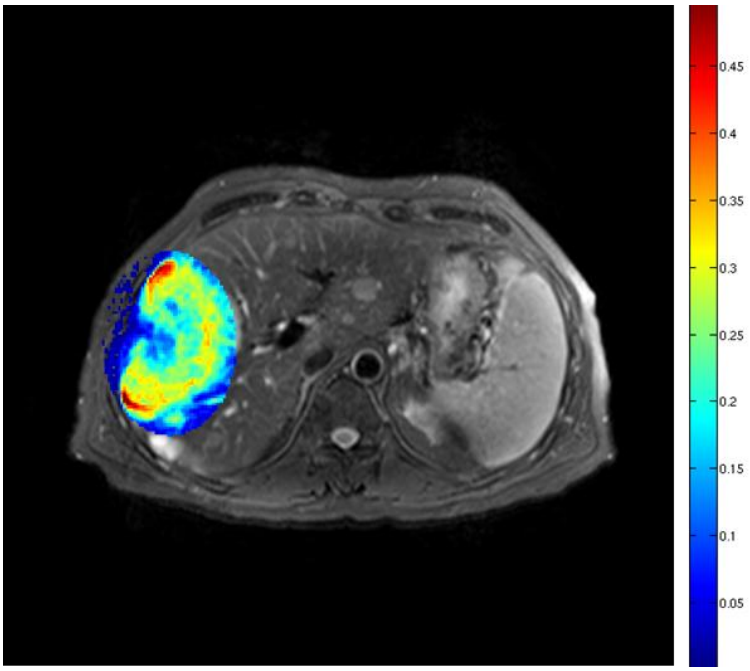

Figure 5. Color map of E_R of the tumor region overlying the same slice of T_2-weighed anatomical image.

Perfusion data of the same ROI in a slice of the tumor were calculated to obtain serial color maps of E_R of the before treatment, and one week, 6 weeks, and 12 weeks after treatment. The histogram distribution of E_R values over the ROI for each study is shown in Figure 6. Patient 3's data, depicted in Figure 6a, reveal that a large population of pixels in the ROI was shifted to lower E_R values after the first treatments and remained at lower values at 6 and 12 weeks after treatments. However, as can be seen in Figure 6b, data from

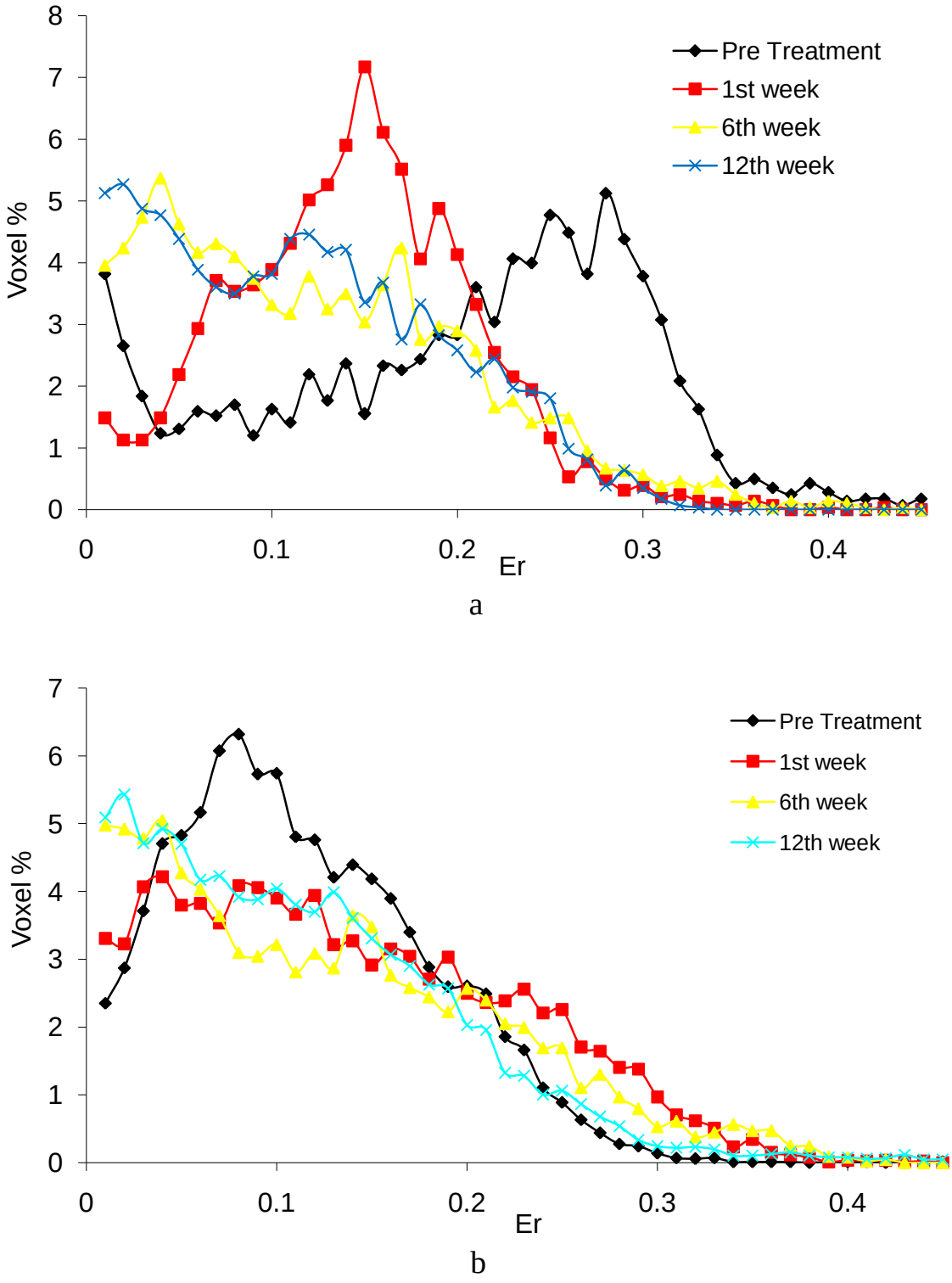

Figure 6. Histograms of E_Rs in tumors. a: From patient 3 data. b: From patient 1 data. Histograms depict data collected before treatment and one week, 6 weeks, and 12 weeks after treatment was started.

another patient (patient 1) showed only a small shift in distribution of E_R after the first treatments.

The E_R and standard deviation were calculated in the selected ROI that covered only the tumor peripheral area. Values of 5 patients from before treatment and from one week and 6 weeks after treatment are plotted in Figure 7. It is shown that the E_R decreased in 3 patients (patients 3, 4, and 5) after the first week of treatment.

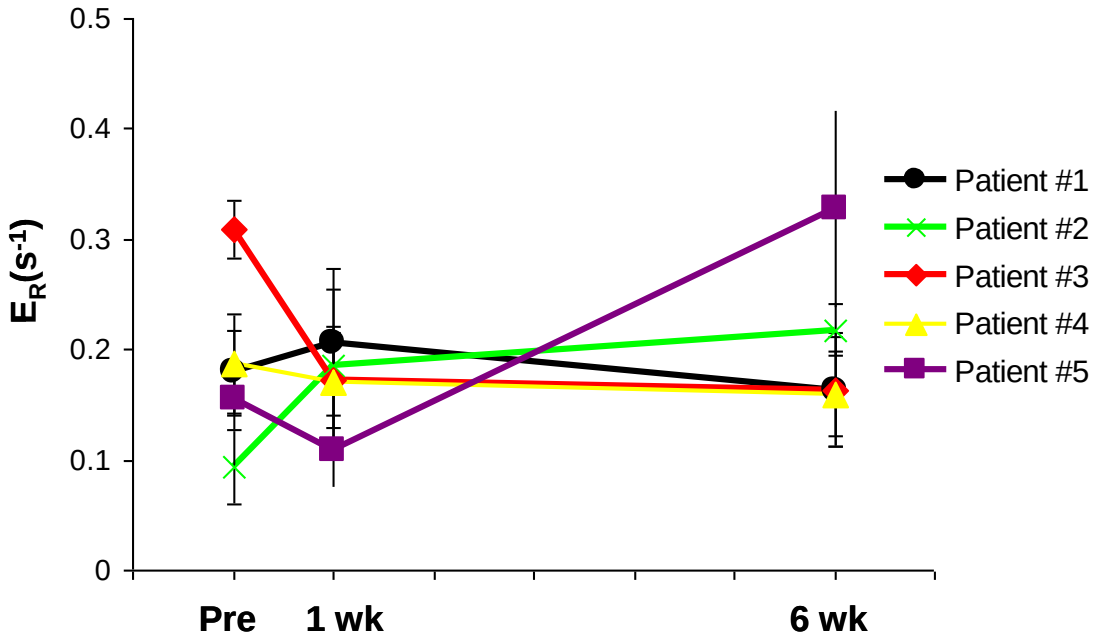

Figure 7. E_Rs of selected ROIs covering tumor peripheral areas before treatment, and one week and 6 weeks after treatment was started. Figure includes rates of all 5 patients studied.

K^{trans} was obtained by fitting the data points from the first 20-30 seconds (acquired during the patient's first breath holding) into the two compartment model discussed in Material and Methods. As was done for the E_R, a color map was generated over the selected ROI covering the whole tumor region. Figure 8 shows K^{trans} color maps of the selected region overlying the respective T_2-weighed images of patient 3. It can be easily seen

that high K^{trans} values of some areas were reduced to low values and appear to be more homogeneous across the tumor lesion after both the first and the 6th weeks of treatments. A histogram of the distribution of K^{trans} values over the tumor region is shown in Figure 9. This patient's (patient 3) data reveal that the K^{trans} values of a large population of pixels were shifted to lower values after the first week treatment and remained low with a larger pixel volume after the 6th week of treatment. These changes can also be seen easily in Figure 8. The K^{trans} values of patients 3, 4, and 5 during treatments are plotted in Figure 10.

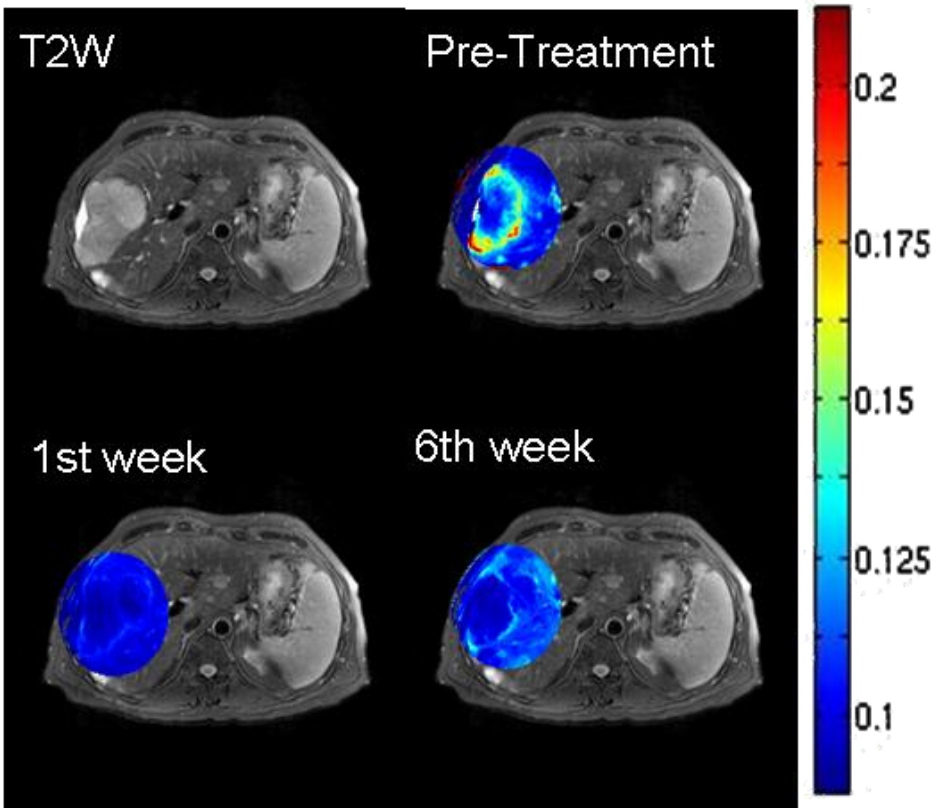

Figure 8. T_2-weighted image and overlying K^{trans} maps of tumor region obtained before treatment and one week and 6 weeks after treatment of patient 3 was started.

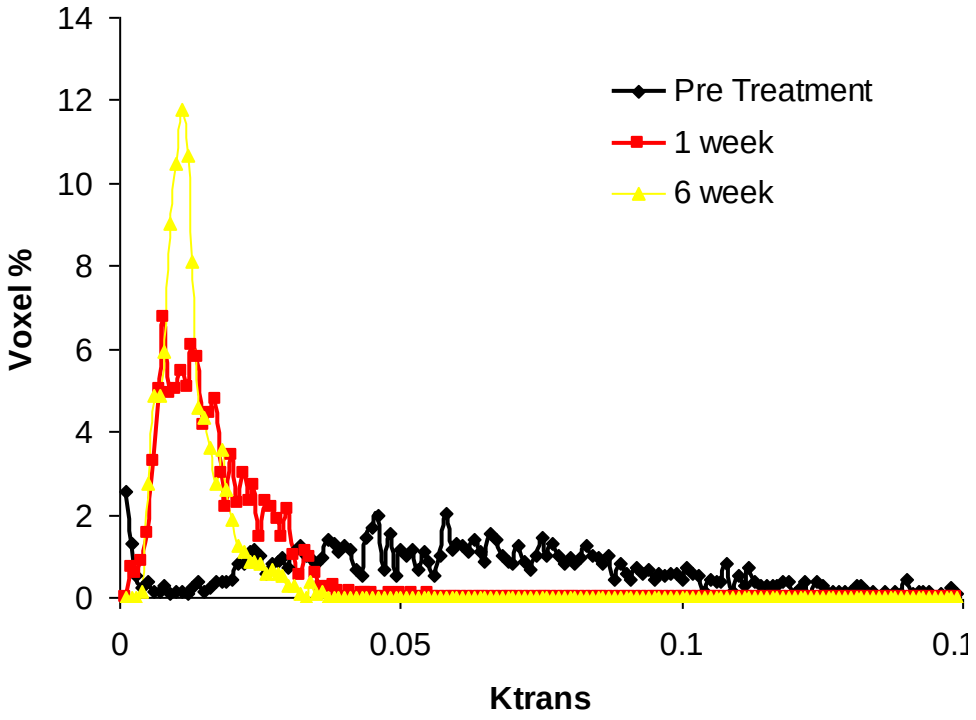

Figure 9. Histograms of K^{trans} before treatment and one week and 6 weeks after treatment of patient 3 was started.

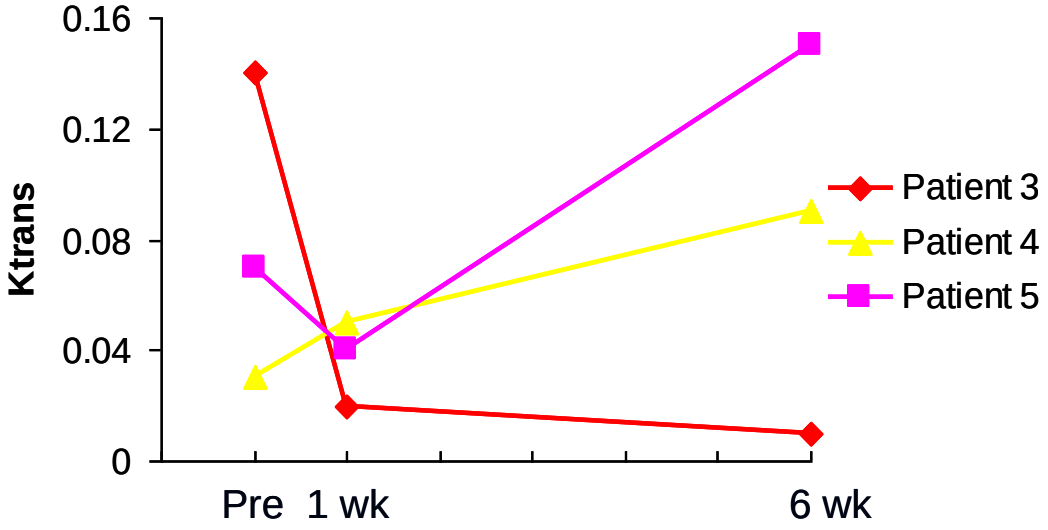

Figure 10. K^{trans} of ROIs covering tumor peripheral areas before treatment and one week and 6 weeks after treatment of patients 3, 4, and 5 was started.

DISCUSSION

DCE-MRI in the human abdomen has been successfully implemented with the use of a Philips 3 T MR scanner. With a phased array body receive coil, a large 3D volume was cquired at rate of 2.1 seconds by a 3D T_1-FFE sequence with SENSE factor 2, which gave enough points to obtain a wash-in curve from the aorta for use in calculating the AIF. In addition, a faster acquisition method made it possible to acquire the whole signal enhancement wash-in curve in one breath hold by increasing the contrast agent injection rate. In our study, we used the signal enhancement curve of the first 20-30 seconds during one breath hold to estimate K^{trans}. This technique enables the acquisition of a sequence of images without motion artifacts, as well as avoids the contribution of potential error from the portal vein flow. The k_{ep} and v_e were not estimated in our study because these parameters are highly sensitive to the potential contribution of the portal vein flow in the current model.

The tumor response to the treatment was monitored in terms of the DCE-MRI parameters K^{trans} and E_R. It was observed that 3 out of 5 patients (patients 3, 4, and 5) showed a reduced E_R after the first week of treatment. The E_R values of patients 3 and 4 continually decreased after 6 weeks of treatment, whereas patient 5 showed an increase in E_R after 6 weeks of treatment. Patient 1 showed a lower E_R value after 6 weeks of treatment, although he showed a higher E_R level after the first week of treatment. In 3 patients, K^{trans} revealed trends similar to those trends for the E_R. Of 5 patients, only patients 1, 2, and 3 received

sorafenib during the therapy. Our data showed a significant effect of this drug in patient 3 in whom the values of E_R and K^{trans} were reduced after one week and 6 weeks of therapy. The E_R value of patient 1 decreased after 6 weeks of treatment, although this value increased slightly after one week of therapy. Both patients showed stable disease in the outcomes of clinical tests. No response to treatment was found for patient 2 in either E_R values or clinical tests during the therapies. Of the 2 patients (patients 4 and 5) who did not receive sorafenib, patient 5 showed decreased values of E_R and K^{trans} after one week of treatment, but both parameters reversely increased at the 6^{th} week; these data suggest that this patient had vascular alteration in response to the chemotherapy during the early stage of treatment.

In our study, the GKM was employed in the calculation of the DCE-MRI pharmacokinetic parameter, K^{trans}. The GKM is a two compartment model with one input function and has been widely used and accepted in DCE-MRI studies (33). Although the liver we studied currently has two vascular supplies, the GKM fitted the data very well when the blood contribution from only the arterial phase and the early part of the signal enhancement curve were used in quantifying pharmacokinetic parameters. Because most organs have one vascular supply, the current setup will be easily applied in other studies to evaluate the treatment of cancers in other organs in clinical trials, such as brain tumor (11), breast tumor (14), and prostate tumor (23). The AIF is required in the GKM to calculate pharmacokinetic parameters. It is important to cover the artery or arterioles in the FOV of acquired DCE-MRI images. In addition, a precontrast T_1 measurement method is needed to optimize the use of DCE-MRI studies of different organs.

Our limited data indicate that DCE-MRI appears to be effective not only as a biomarker for evaluating the antiangiogenic therapy but also as a method of detecting the vascular response to the systemic therapies. Previous work by Browder et al. (39) has shown that systemic chemotherapy may have an antiangiogenic effect when administered at concentrations far below the established maximum tolerated doses because it works as a nonselective antiangiogenic agent by exerting antiproliferative, anti-invasive, or cytotoxic effects on multiple cell types, including angiogenic endothelial cells (40). In addition, because of the pharmacokinetic model used in this study, the treatment response indicated by the decreasing E_R or K^{trans} values that we observed in these patients may also reflect changes in the regional blood flow and surface area of endothelial membrane; these changes may be caused by the antiangiogenic drug sorafenib but also by the chemotherapy.

Workie et al. (32) showed that the E_R is proportional to the K^{trans}.

$$E_R = T_{10} r_1 C_{p0} K^{trans} \qquad (9)$$

if it is assumed that the concentration of contrast agent immediately reaches equilibrium. In our study, K^{trans} and E_R are highly correlated with each other (R = 0.8178; see Figure 11). The E_R is generally easier to measure and can show the perfusion condition in a tumor because the E_R ignores the dynamic concentration change in the plasma, which perfuses the contrast agent into the tissue. The AIF may not only vary among patients but also have different shapes for a given patient in different study sessions. For DCE-MRI in the liver, the AIF will be more critical because the liver has a dual vascular input, and the contribution from the hepatic artery and the portal vein may vary in different liver diseases and at different time points of treatment. In our study, the E_R revealed response trends similar to those of the K^{trans} in all patients but patient 4, whose data showed a decrease in E_R values

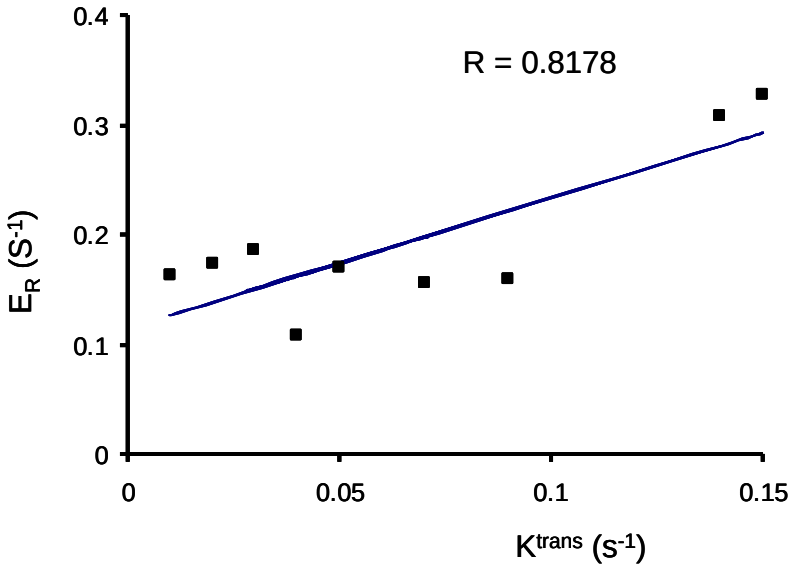

Figure 11. The relationship between K^{trans} and E_R.

but an increase in K^{trans} values throughout the therapy. Most patients in our study showed similar AIFs at each MRI study, and this result corresponds to the similar trends seen in the E_R and K^{trans}. However, patient 4 had different AIFs for each MRI session (data not shown inthesis); this resulted in different magnitudes of enhancement.

Currently, the time to progression is the major end point of most clinical trials of antiangiogenic compounds. DCE-MRI has the potential to serve as the end point in these clinical studies. However, current pharmacokinetic modeling of DCE-MRI gives mixed information about the vessel permeability, the vascular flow, and the surface area of the vessel membrane; as a result, DCE-MRI at the present time can be only a relative bio-marker with which to monitor the treatment response and cannot be an end point for de-termining an antiangiogenesis effect of agents such as the tyrosine kinase inhibitor sora-fenib. Choosing a pharmacokinetic model in DCE-MRI is always a compromise between accuracy and computational complexity. Further development of the modeling of contrast

agent kinetics will be the most important task involved in to accurately evaluating the antiangiogenic treatment.

LIST OF REFERENCES

1. Parkin DM, Pisani P, Ferlay J. Estimates of the worldwide incidence of 25 major cancers in 1990. Int J Cancer 1999;80(6):827-841.

2. Bruix J, Sherman M, Llovet JM, Beaugrand M, Lencioni R, Burroughs AK, Christensen E, Pagliaro L, Colombo M, Rodes J. Clinical management of hepatocellular carcinoma. Conclusions of the Barcelona-2000 EASL conference. European Association for the Study of the Liver. J Hepatol 2001;35(3):421-430.

3. Llovet JM, Bruix J, Gores GJ. Surgical resection versus transplantation for early hepatocellular carcinoma: clues for the best strategy. Hepatology 2000;31(4): 1019-1021.

4. Beaugrand M, N'Kontchou G, Seror O, Ganne N, Trinchet JC. Local/regional and systemic treatments of hepatocellular carcinoma. Semin Liver Dis 2005;25(2): 201-211.

5. Folkman J. Tumor angiogenesis: therapeutic implications. N Engl J Med 1971;285(21):1182-1186.

6. D'Angelo G, Struman I, Martial J, Weiner RI. Activation of mitogen-activated protein kinases by vascular endothelial growth factor and basic fibroblast growth factor in capillary endothelial cells is inhibited by the antiangiogenic factor 16-kDa N-terminal fragment of prolactin. Proc Natl Acad Sci U S A 1995;92(14): 6374-6378.

7. Landgren E, Schiller P, Cao Y, Claesson-Welsh L. Placenta growth factor stimulates MAP kinase and mitogenicity but not phospholipase C-gamma and migration of endothelial cells expressing Flt 1. Oncogene 1998;16(3):359-367.

8. Waltenberger J, Claesson-Welsh L, Siegbahn A, Shibuya M, Heldin CH. Different signal transduction properties of KDR and Flt1, two receptors for vascular endothelial growth factor. J Biol Chem 1994;269(43):26988-26995.

9. Choyke PL, Dwyer AJ, Knopp MV. Functional tumor imaging with dynamic contrast-enhanced magnetic resonance imaging. J Magn Reson Imaging 2003; 17(5):509-520.

10. Brix G, Semmler W, Port R, Schad LR, Layer G, Lorenz WJ. Pharmacokinetic parameters in CNS Gd-DTPA enhanced MR imaging. J Comput Assist Tomogr 1991;15(4):621-628.

11. Larsson HB, Stubgaard M, Frederiksen JL, Jensen M, Henriksen O, Paulson OB. Quantitation of blood-brain barrier defect by magnetic resonance imaging and gadolinium-DTPA in patients with multiple sclerosis and brain tumors. Magn Reson Med 1990;16(1):117-131.

12. Weindel K, Moringlane JR, Marme D, Weich HA. Detection and quantification of vascular endothelial growth factor/vascular permeability factor in brain tumor tissue and cyst fluid: the key to angiogenesis? Neurosurgery 1994;35(3):439-448.

13. Zhu XP, Li KL, Kamaly-Asl ID, Checkley DR, Tessier JJ, Waterton JC, Jackson A. Quantification of endothelial permeability, leakage space, and blood volume in brain tumors using combined T1 and T2* contrast-enhanced dynamic MR imaging. J Magn Reson Imaging 2000;11(6):575-585.

14. Daldrup HE, Shames DM, Husseini W, Wendland MF, Okuhata Y, Brasch RC. Quantification of the extraction fraction for gadopentetate across breast cancer capillaries. Magn Reson Med 1998;40(4):537-543.

15. Port RE, Knopp MV, Hoffmann U, Milker-Zabel S, Brix G. Multicompartment analysis of gadolinium chelate kinetics: blood-tissue exchange in mammary tumors as monitored by dynamic MR imaging. J Magn Reson Imaging 1999;10(3): 233-241.

16. Devries AF, Griebel J, Kremser C, Judmaier W, Gneiting T, Kreczy A, Ofner D, Pfeiffer KP, Brix G, Lukas P. Tumor microcirculation evaluated by dynamic magnetic resonance imaging predicts therapy outcome for primary rectal carcinoma. Cancer Res 2001;61(6):2513-2516.

17. Barentsz JO, Engelbrecht M, Jager GJ, Witjes JA, de LaRosette J, van Der Sanden BP, Huisman HJ, Heerschap A. Fast dynamic gadolinium-enhanced MR imaging of urinary bladder and prostate cancer. J Magn Reson Imaging 1999;10(3): 295-304.

18. Mayr NA, Hawighorst H, Yuh WT, Essig M, Magnotta VA, Knopp MV. MR microcirculation assessment in cervical cancer: correlations with histomorphological tumor markers and clinical outcome. J Magn Reson Imaging 1999;10(3):267-276.

19. van Laarhoven HW, Rijpkema M, Punt CJ, Ruers TJ, Hendriks JC, Barentsz JO, Heerschap A. Method for quantitation of dynamic MRI contrast agent uptake in colorectal liver metastases. J Magn Reson Imaging 2003;18(3):315-320.

20. Barentsz JO, Berger-Hartog O, Witjes JA, Hulsbergen-van der Kaa C, Oosterhof GO, VanderLaak JA, Kondacki H, Ruijs SH. Evaluation of chemotherapy in advanced urinary bladder cancer with fast dynamic contrast-enhanced MR imaging. Radiology 1998;207(3):791-797.

21. van Laarhoven HW, Klomp DW, Rijpkema M, Kamm YL, Wagener DJ, Barentsz JO, Punt CJ, Heerschap A. Prediction of chemotherapeutic response of colorectal liver metastases with dynamic gadolinium-DTPA-enhanced MRI and localized (19)F MRS pharmacokinetic studies of 5-fluorouracil. NMR Biomed 2006.

22. Hawighorst H, Knopp MV, Debus J, Hoffmann U, Grandy M, Griebel J, Zuna I, Essig M, Schoenberg SO, DeVries A, Brix G, van Kaick G. Pharmacokinetic MRI for assessment of malignant glioma response to stereotactic radiotherapy: initial results. J Magn Reson Imaging 1998;8(4):783-788.

23. Padhani AR, MacVicar AD, Gapinski CJ, Dearnaley DP, Parker GJ, Suckling J, Leach MO, Husband JE. Effects of androgen deprivation on prostatic morphology and vascular permeability evaluated with mr imaging. Radiology 2001;218(2): 365-374.

24. Posey JA, Ng TC, Yang B, Khazaeli MB, Carpenter MD, Fox F, Needle M, Waksal H, LoBuglio AF. A phase I study of anti-kinase insert domain-containing receptor antibody, IMC-1C11, in patients with liver metastases from colorectal carcinoma. Clin Cancer Res 2003;9(4):1323-1332.

25. Leach MO, Brindle KM, Evelhoch JL, Griffiths JR, Horsman MR, Jackson A, Jayson GC, Judson IR, Knopp MV, Maxwell RJ, McIntyre D, Padhani AR, Price P, Rathbone R, Rustin GJ, Tofts PS, Tozer GM, Vennart W, Waterton JC, Williams SR, Workman P. The assessment of antiangiogenic and antivascular therapies in early-stage clinical trials using magnetic resonance imaging: issues and recommendations. Br J Cancer 2005;92(9):1599-1610.

26. Carmeliet P, Jain RK. Angiogenesis in cancer and other diseases. Nature 2000;407(6801):249-257.

27. Padhani AR. Dynamic contrast-enhanced MRI in clinical oncology: current status and future directions. J Magn Reson Imaging 2002;16(4):407-422.

28. Knopp MV, Weiss E, Sinn HP, Mattern J, Junkermann H, Radeleff J, Magener A, Brix G, Delorme S, Zuna I, van Kaick G. Pathophysiologic basis of contrast enhancement in breast tumors. J Magn Reson Imaging 1999;10(3):260-266.

29. Oesterle C, Strohschein R, Kohler M, Schnell M, Hennig J. Benefits and pitfalls of keyhole imaging, especially in first-pass perfusion studies. J Magn Reson Imaging 2000;11(3):312-323.

30. Tsao J, Boesiger P, Pruessmann KP. k-t BLAST and k-t SENSE: dynamic MRI with high frame rate exploiting spatiotemporal correlations. Magn Reson Med 2003;50(5):1031-1042.

31. Haacke EM, Brown RW, Thompson MR, R. V. Magnetic resonance imaging: physical principles and sequence design.: Wiley-Liss; 1999.

32. Workie DW, Dardzinski BJ, Graham TB, Laor T, Bommer WA, O'Brien KJ. Quantification of dynamic contrast-enhanced MR imaging of the knee in children with juvenile rheumatoid arthritis based on pharmacokinetic modeling. Magn Reson Imaging 2004;22(9):1201-1210.

33. Tofts PS, Brix G, Buckley DL, Evelhoch JL, Henderson E, Knopp MV, Larsson HB, Lee TY, Mayr NA, Parker GJ, Port RE, Taylor J, Weisskoff RM. Estimating kinetic parameters from dynamic contrast-enhanced T(1)-weighted MRI of a diffusable tracer: standardized quantities and symbols. J Magn Reson Imaging 1999;10(3):223-232.

34. Tofts PS, Kermode AG. Measurement of the blood-brain barrier permeability and leakage space using dynamic MR imaging. 1. Fundamental concepts. Magn Reson Med 1991;17(2):357-367.

35. Materne R, Smith AM, Peeters F, Dehoux JP, Keyeux A, Horsmans Y, Van Beers BE. Assessment of hepatic perfusion parameters with dynamic MRI. Magn Reson Med 2002;47(1):135-142.

36. Liu L, Cao Y, Chen C, Zhang X, McNabola A, Wilkie D, Wilhelm S, Lynch M, Carter C. Sorafenib blocks the RAF/MEK/ERK pathway, inhibits tumor angiogenesis, and induces tumor cell apoptosis in hepatocellular carcinoma model PLC/PRF/5. Cancer Res 2006;66(24):11851-11858.

37. Richly H, Henning BF, Kupsch P, Passarge K, Grubert M, Hilger RA, Christensen O, Brendel E, Schwartz B, Ludwig M, Flashar C, Voigtmann R, Scheulen ME, Seeber S, Strumberg D. Results of a Phase I trial of sorafenib (BAY 43-9006) in combination with doxorubicin in patients with refractory solid tumors. Ann Oncol 2006;17(5):866-873.

38. Abou-Alfa GK, Schwartz L, Ricci S, Amadori D, Santoro A, Figer A, De Greve J, Douillard JY, Lathia C, Schwartz B, Taylor I, Moscovici M, Saltz LB. Phase II study of sorafenib in patients with advanced hepatocellular carcinoma. J Clin Oncol 2006;24(26):4293-4300.

39. Browder T, Butterfield CE, Kraling BM, Shi B, Marshall B, O'Reilly MS, Folkman J. Antiangiogenic scheduling of chemotherapy improves efficacy against experimental drug-resistant cancer. Cancer Res 2000;60(7):1878-1886.

40. Vogler WR LJ, Volpert O, Adres EW, Bouck N. The anticancer drug edelfosine is a potent inhibitor of neovascularization in vivo. Cancer Invest 1998;16:549-553.

APPENDIX

INSTITUTIONAL REVIEW BOARD FOR HUMAN USE APPROVAL FORM

THE UNIVERSITY OF ALABAMA AT BIRMINGHAM

Institutional Review Board for Human Use

Form 4: IRB Approval Form
Identification and Certification of Research
Projects Involving Human Subjects

UAB's Institutional Review Boards for Human Use (IRBs) have an approved Federalwide Assurance with the Office for Human Research Protections (OHRP). The UAB IRBs are also in compliance with 21 CFR Parts 50 and 56 and ICH GCP Guidelines. The Assurance became effective on November 24, 2003 and expires on February 14, 2009. The Assurance number is FWA00005960.

Principal Investigator: JIANG, YUN

Co-Investigator(s):

Protocol Number: **X061213008**

Protocol Title: *Assessment of Dynamic Contrast Enhanced MRI for the Early Detection of Treatment Response in Human Advanced Hepatocellular Carcinoma at 3T*

The IRB reviewed and approved the above named project on 12/15/06. The review was conducted in accordance with UAB's Assurance of Compliance approved by the Department of Health and Human Services. This Project will be subject to Annual continuing review as provided in that Assurance.

This project received EXPEDITED review.

IRB Approval Date: 12-15-06

Date IRB Approval Issued: 12/15/06

Marilyn Doss

Marilyn Doss, M.A.
Vice Chair of the Institutional Review Board for Human Use (IRB)

Investigators please note:

The IRB approved consent form used in the study must contain the IRB approval date and expiration date.

IRB approval is given for one year unless otherwise noted. For projects subject to annual review research activities may not continue past the one year anniversary of the IRB approval date.

Any modifications in the study methodology, protocol and/or consent form must be submitted for review and approval to the IRB prior to implementation.

Adverse Events and/or unanticipated risks to subjects or others at UAB or other participating institutions must be reported promptly to the IRB.

470 Administration Building
701 20th Street South
205.934.3789
Fax 205.934.1301
irb@uab.edu

The University of
Alabama at Birmingham
Mailing Address:
AB 470
1530 3RD AVE S
BIRMINGHAM AL 35294-0104